Published by :
http://www.ijert.org

International Journal of Engineering Research & Technology (IJERT)
ISSN: 2278-0181
Vol. 9 Issue 04, April-2020

MPC-based Droop Control of Parallel Inverters for Voltage and Frequency Stabilization in Autonomous AC Microgrid

Jean De Dieu Iyakaremye
PhD Scholar,
Dept. of EE PAUSTI
Nairobi, Kenya

George N. Nyakoe
Associate Professor,
College of Engineering and Technology JKUAT
Nairobi, Kenya

Cyrus W. Wekesa
Associate Professor,
Dept. of EE
PAUSTI Nairobi-Kenya

***Abstract*— Over the years, the production and use of renewable energy sources (RES) based on solar, wind and other clean energy sources have gained growing public attention in addressing problems of energy shortage and environmental pollution resulting from conventional fossil fuels. The incorporation of electronic power converters into the grid involves a significant number of RES which suggests that the future grid must consist of RES, storage and loads interfaced with electronic power converters. In stand-alone microgrids based on voltage source inverters (VSI), control issues are the main challenges due to the low inertia, uncertainty and intermittent nature of RES. To solve this problem, an adequate control strategy is needed to stabilize voltage and frequency, ensuring power supply and managing intermittence. This paper proposes the predictive control model for the inverter based on the virtual resistance droop control technique and restorative control strategy. The proposed control strategy showed good results in stabilizing the voltage and the frequency in allowable limits of +/-10% and +/-5% respectively. It has found that the control strategy helps the microsources to share the power adequately. Simulation tests demonstrate the precision and efficacy of the suggested control technique.**

Keywords*— Droop control, model predictive control, microgrids, Voltage source inverter, parallel inverters, voltage and frequency stabilization, power-sharing.

I. INTRODUCTION

Distributed generation (DG) of sustainable power source based frameworks, for example, photovoltaic and wind, joined with load and electricity storage systems, is acquainting transformative changes with regular utilities and is turning into another network model. The possibility of microgrids (MG) is rising as opposed to traditional generators as a successful method for consolidating sustainable power sources [1].

A typical MG is comprised of interconnected DG which shapes a key square element. MGs are picking up ubiquity because of their flexibility and having the option to work in two essential modes: islanded and grid-connected. Numerous kinds of DGs, for example, miniaturized scale turbines, photovoltaic systems, and electricity storage systems should be connected by power electronic gadgets with MG, permitting them to work and being controlled more adaptable. Nevertheless, the MG is inherently vulnerable to grid instability due to its physical insignificance inertia [2].

This power electronic gadget interface can be a current source inverter (CSI) used to infuse current into the connected grid; the inverter is controlled to fulfill an assured real and reactive power setting level. This is applied when the inverter has to share real and reactive power with the grid. The power electronic gadget can also be a voltage source inverter (VSI) linked in parallel to form an independent or isolated micro-grid, i.e. suitable for driving a local load, for example in motor drives or isolated systems where the inverter is the only source of power [3].

VSI's parallel design allows multiple voltage source inverters to be connected to form a microgrid, thereby allowing production cost savings and enabling network expansion to increase the efficiency and reliability of power supply systems. Any DG is expected to meet the following requirements in autonomous mode [4]: 1) Any DG operating mode switching should not affect the steady-state operation of the microgrid; 2) The DG should autonomously control its frequency and voltage according to the local DG information itself. The proper controller design is very critical for this configuration to achieve the correct sharing of loads between all types of sources. Current literature has documented many centralized microgrid control techniques based on external communication links between the inverters. Such controllers create a technical and economic barrier, in particular for remote microgrids [5].

The utilization of the droop control approach is preferred because of its capability to control the power exchange and there are no additional communication facilities needed among the connected voltage source inverters. On the side of power-sharing, the traditional droop control's transient response is slow, and the deviations of frequency/voltage are high. These factors restrict the exact power-sharing between the inverters with parallel connections.

There exist numerous droop control strategies discussed in the literature for proper power sharing for linear and/or non-linear loads. The standard stationary control uses active power / frequency (P / f) and reactive power / voltage (Q / V) control to control active and reactive power decoupling [6], [7], [8], [9], [10], [11], [12], and [13].

International Journal of Engineering Research & Technology (IJERT)
ISSN: 2278-0181
Vol. 9 Issue 04, April-2020

This paper introduces a droop control strategy based on the MPC (model predictive control) with voltage and frequency restorative loops for the good operation of parallel linked inverters in an AC microgrid. The suggested control strategy will increase the transient response, reach greater reactive and active power capacity, and substantially reduce variations in voltage and frequency. To avoid overload of parallel-connected microsources and to ensure the sharing of power among the DGs, every inverter's controls should be managed in such a way that each microsource satisfies the load demand based on the power rating of the DG [1].

Distributed energy resources (DER) systems can work under three different conditions in interconnected grid ac microgrids. These are called grid-forming units, grid-feeding units, and grid-supporting units. Authors in [14] describe the DER device control approaches according to the operating conditions.

This paper is divided into five main parts. After presenting the structure of the microgrid functions and operating conditions, resistance droop control and model predictive control strategies were presented in part II. The proposed MPC-based droop control approach is discussed in part III. In part IV, the performance analysis of the proposed droop control is reported and simulation results are discussed. Part V presents the conclusion.

II. MICROGRID STRUCTURE AND EXISTING CONTROL STRATEGIES

The arrangement of the microgrid (MG) used is shown in Fig.1. Two DGs are included in this MG. The LC filters and output impedances link each DG with its load. We assume the MG works in an islanded mode.

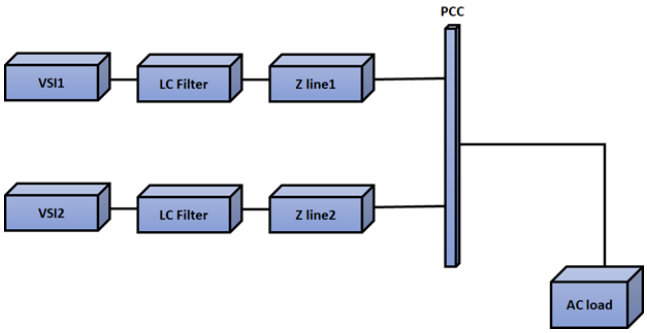

Fig. 1. Microgrid-based inverter systems supplying a common load

A. *Model predictive control*

Three-stage, two-stage, voltage source inverter (VSI), comprising of three legs and an LC filter as portrayed by Figure 2. There are two switches on the leg with two potential exchanging states. The mix of three legs makes eight various conceivable exchanging states, as demonstrated in equation (1).

$$V_t = \frac{2}{3} V_{dc} e^{i(j-1)\left(\frac{\pi}{3}\right)} \quad (j = 0, \ldots, 7) \tag{1}$$

Where V_{dc} is the direct current (DC) source for VSI

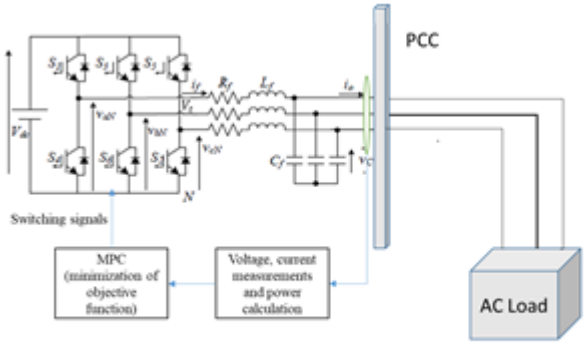

Fig. 2. VSI linked to the AC load

The exchanging states of a diverse combination of voltage vectors can be stated: 000, 100, 110, 010, 011, 001, 101 and 111. In this approach, the DG output voltage and frequency are controlled. The system's mathematical model is obtained from the following equations:

$$i_c = i_f - i_o \tag{2}$$

$$v_c = v_{PC} \tag{3}$$

$$V_t = v_{PC} + v_f + i_f R_f \tag{4}$$

In equation 4, i_c is current flowing in the filter capacitor i_f and i_o are the currents flowing in filter inductor and load respectively. In (4), V_t is the VSI output voltage, v_c is the capacitor voltage, v_{PC} is the voltage at the point of common coupling (PC) and v_f is the filter inductor voltage [12]. The continuous-time state-space model of the system can be written as

$$\frac{dx}{dt} = Ax + B_1 V_t + B_2 i_o \tag{5}$$

Where

$$x = \begin{bmatrix} i_f \\ v_{PC} \end{bmatrix}, \quad A = \begin{bmatrix} \frac{-R_f}{L_f} & \frac{-1}{L_f} \\ \frac{1}{C_f} & 0 \end{bmatrix}, \quad B_1 = \begin{bmatrix} \frac{1}{L_f} \\ 0 \end{bmatrix}, \quad B_2 = \begin{bmatrix} 0 \\ \frac{-1}{C_f} \end{bmatrix}$$

The discrete-time form can be obtained as

$$x(k+1) = A_d x(k) + B_{1d} V_t(k) + B_{2d} i_o(k) \tag{6}$$

Where

$$A_d = e^{AT_s}, \quad B_{1d} = \int_0^{T_s} e^{A\tau} B_1 d\tau, \quad B_{2d} = \int_0^{T_s} e^{A\tau} B_2 d\tau$$

and for a very small sampling time T_s, we estimated the exponential matrix by Taylor series and we get

$$e^{AT_s} \cong 1 + AT_s \tag{7}$$

Using (5), (6) and (7), the future value of the capacitor

International Journal of Engineering Research & Technology (IJERT)
ISSN: 2278-0181
Vol. 9 Issue 04, April-2020

voltage can be predicted by

$$v_{PC}(k+1) = v_{PC}(k) + \frac{T_s}{C_f}\left(i_f(k) - i_o(k)\right) \quad (8)$$

And the cost function in dq reference is given by

$$g_{p,i} = \left(v^*_{PC,d} - v_{PC,d}(k+1)\right)^2 + \left(v^*_{PC,q} - v_{PC,q}(k+1)\right)^2 \quad (9)$$

This cost function is utilized to minimize the error between the reference and predicted voltage values at the PC and to find the optimal value of the voltage vector that should be synthesized at the output of the VSI, where $v_{PC,d}(k+1)$ and $v_{PC,q}(k+1)$ are one step prediction components of v_{pc} measured at PCC in dq reference frames while $v^*_{PC,d}$ and $v^*_{PC,q}$ are the components of reference voltage v^*_{pc} in dq reference frames [11]. Therefore, this cost function assesses every conceivable voltage vector and chooses the one that will limit the error, then the optimum value V_t is produced at the inverter output. Then, the controller will utilize this voltage to produce the necessary switching states for the VSI as expressed by equation 1 and the algorithm used is shown in figure 3.

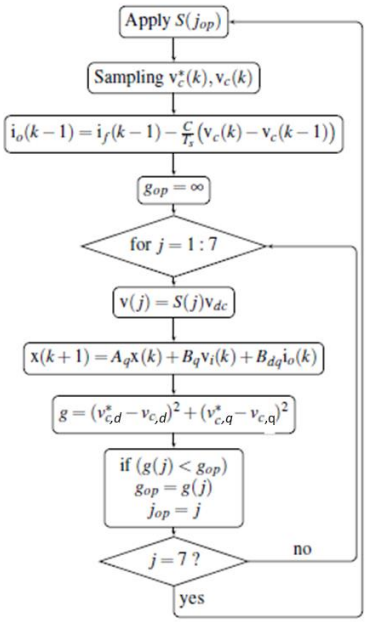

Fig. 3. Algorithm for the selection of switches using MPC in a VSI

B. MPC regulated multiple parallel-connected VSIs in AC microgrid

A single line diagram of the two VSIs linked in parallel to the common coupling via power lines $Z_{oi} = R_{oi} + jX_{oi}$ as depicted in figure 4 is going to be considered in this paper.

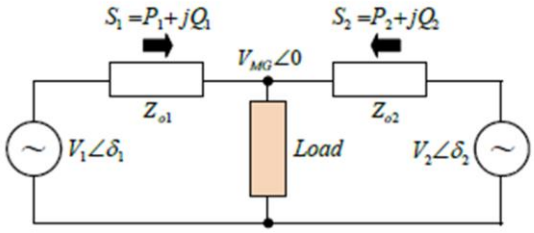

Fig. 4. Two VSIs connected to a common AC microgrid bus

For the proper design of adequate control strategy, the notion of power exchange between the parallel-connected VSI s and PCC as shown in figure 4 is very important. The exchange of power depends on the outputs impedance of each inverter as well as its power rating, the equations which link the later ones are discussed in [15].

$$P_i = \frac{V_i}{R_{oi}^2 + X_{oi}^2}\left[R_{oi}\left(V_i - V_{MG}\cos\delta_i\right) + X_{oi}V_{MG}\sin\delta_i\right] \quad (10)$$

$$Q_i = \frac{V_i}{R_{oi}^2 + X_{oi}^2}\left[-R_{oi}V_{MG}\sin\delta_i + X_{oi}\left(V_i - V_{MG}\cos\delta_i\right)\right] \quad (11)$$

Where V_i and V_{MG} are the amplitudes of the VSI and the bus voltage, respectively, whereas δ_i representing power angles. This is shown in equations (10), (11) where active and reactive power exchange is influenced by both V_i and δ_i, and therefore, it is not possible to control them separately. A generally accepted answer to this problem is to force the output impedance of every VSI to be purely inductive or resistive using different control strategies. The later one is termed as the virtual impedance concept in the literature [16].

C. Virtual Impedance Loop

The authors in [17] reveal that the virtual resistive impedance is preferable than virtual inductive impedance since the virtual resistive impedance is not depending on frequency. This makes the later one especially appropriate for the power-sharing and transient conditions of nonlinear loads. Furthermore, it is considered to add the damping capability to the system thus desirable from an MG stability point of view. The virtual resistive impedance control loop is carried out as follows:

$$v^*_{ref} = v_{ref} - R_v i_o \quad (12)$$

Where R_v is the resistive impedance, v^*_{ref} is the voltage reference after virtual impedance loop to be used in the cost function, while v_{ref} is the voltage reference obtained from droop control, which is explained in the next subsection.

When the R_v is set high enough so that the output impedance becomes dominantly resistive, and assuming of small-angle δ_i between the voltage at VSI and MG ends, it can be stated that $X_{oi} \approx 0$, $\sin\delta_i \approx \delta_i$ and $\cos\delta_i \approx 1$ in (10)-(11). This leads to the following set of equations:

International Journal of Engineering Research & Technology (IJERT)
ISSN: 2278-0181
Vol. 9 Issue 04, April-2020

$$P_i = \frac{V_i}{R_{oi}}\left(V_i - V_{MG}\right) \quad (13)$$

$$Q_i = -\frac{V_i V_{MG}}{R_{oi}}\delta_i \quad (14)$$

It is now easy to note that the active power exchange is controlled by $\Delta V = V_i - V_{MG}$ while the reactive power is controlled by the power angle δ_i .

D. Droop Control Strategy

Taking into consideration of equations (13)-(14), droop control can be designed as follows:

$$v_{ref} = v_{nom} - m_p P_{cal} \quad (15)$$

$$\omega_{ref} = \omega_{nom} + n_q Q_{cal} \quad (16)$$

Where v_{ref} and ω_{ref} represent the amplitude of reference voltage and frequency used to calculate v^*_{ref} while v_{nom} and ω_{nom} are nominal voltage amplitude and frequency, respectively. Droop coefficients m_p and n_q determine the slope of the droop curves and respectively, voltage descents and frequency increases for given working conditions. These quantities are usually chosen in ratio to the power rating of VSIs. Finally P_{cal} and Q_{cal} are respectively instantaneous active and reactive power, which are computed as:

$$P_{cal} = v_{PC,d} i_{o\alpha} + v_{PC,q} i_{oq} \quad (17)$$

$$Q_{cal} = v_{PC,q} i_{od} - v_{PC,d} i_{oq} \quad (18)$$

Powers measured in (17)-(18) will pass through low-pass filters before being applied to (15)-(16) [18].

III. THE PROPOSED VOLTAGE AND FREQUENCY STABILIZATION CONTROL STRATEGY

The VSI in autonomous microgrid works principally in grid forming mode. The decoupled control of active power (P) and reactive power (Q) are obtained under the synchronous reference frame utilizing voltage vector-based control. Meanwhile, in this reference frame, the control variables enable the implementation of a virtual impedance control strategy, the model predictive control, and the restorative control strategies. The proposed block diagram for the control strategy is displayed in figure 5. The structure of multi loops is applied including droop control, resistance virtual impedance, restorative control and model predictive control, and the complete control blocks are presented in figures 6, 7, 8 and 9 respectively. Figure 5 illustrates the procedure for the systematic implementation of the control strategy for typical VSI integrated with MG.

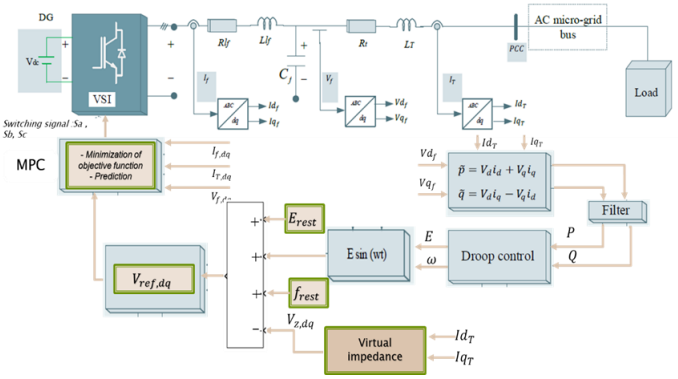

Fig. 5. Control strategy of voltage and frequency stabilization

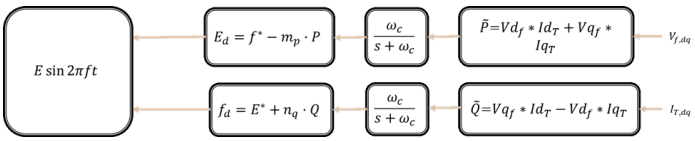

Fig. 6. Droop control block

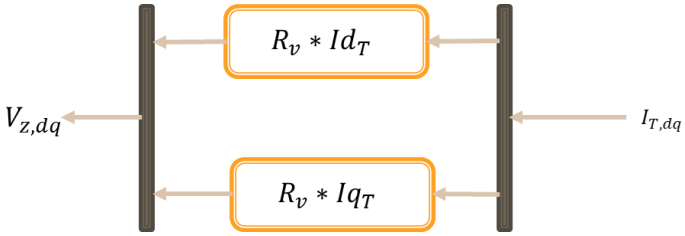

Fig. 7. Virtual resistance control block

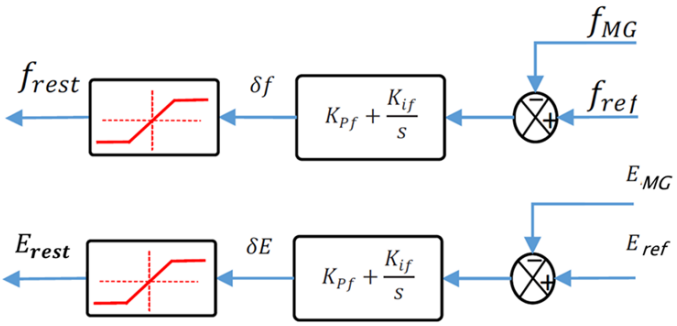

Fig. 8. Restorative control block

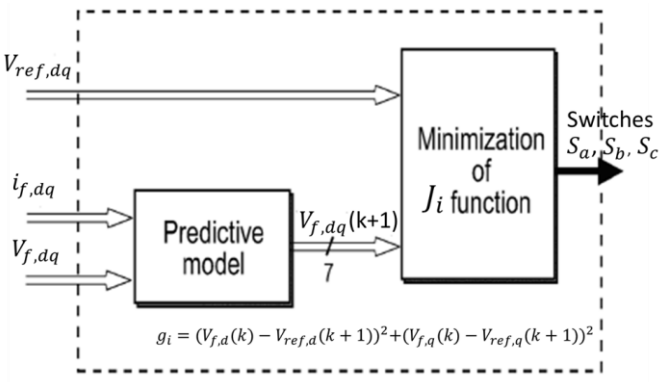

Fig. 9. Predictive control block

International Journal of Engineering Research & Technology (IJERT)
ISSN: 2278-0181
Vol. 9 Issue 04, April-2020

Where the $V_{f,dq}$ is filter capacitor voltage and $V_{ref,dq}$ is the voltage obtained after the implementation of the droop, virtual resistance and restorative control blocks. The predictive model of each VSI is implemented in the same way as indicated in equations (1)-(9) and the switching states are selected using the algorithm presented in figure 3.

IV. RESULTS AND DISCUSSION

A detailed simulation for both single and parallel-operated inverter (VSI) using MATLAB / Simulink has been performed for the validation of the output of the suggested controller for the VSI based microgrid system. Figure 1 shows the system studied in this work. The test-system parameters are given in Table 1.

Table 1: Test system parameters

Parameter	Value
DC link voltage	$Vdc = 520\ V$
Sample time	$Ts = 30\mu s$
LC filter	$L_f = 2.4mH,\ C_f = 25\mu F$
Linear loads	$R_1 = 33\Omega,\ L_1 = 7mH$ $R_2 = 10\Omega,\ L_2 = 3.5mH$
Nonlinear loads	$R_n = 70\Omega,\ C_n = 1100\mu F$
Nominal voltage	$V_{nom} = 230V,\ f_{nom} = 50Hz$
Droop coefficients	$m_p = 0.001\ ^{V}/_{W},\ n_q = 0.001\ ^{rad}/_{sVar}$
Line impedance	$R_{oi} = 0.1\Omega,\ L_{oi} = 2.4mH$
Virtual impedance	$R_v = 2\Omega$
Voltage restoration terms	$K_{pVrest} = 15e-4,\ K_{iVrest} = 500$
Frequency restoration terms	$K_{pfrest} = 15e-4,\ K_{ifrest} = 1000$

In various simulation instances, the robustness and reliability of the proposed controller were demonstrated. Next, a steady-state simulation for one inverter was performed to check the efficacy of the suggested controller under the reference for sinusoidal voltage. A transient response, load step change and system response were then examined under nonlinear load. The results indicated that the controller offers adequate control capabilities to the system. Finally, the proposed controller has been used in a setup of two VSI connected in parallel. A proper power-sharing has been achieved by using the proposed control strategies as shown by figures 20 and 21.

A. Steady-state analysis

Figures 10 and 12 show the voltage and frequency variation of the single VSI supplied linear load and nonlinear load respectively underbalanced condition. The reference of phase voltage and voltage reference was set at 230 V and 50Hz. Output voltage and current waveforms were sinusoidal at small harmonic distortions. During our study, a linear RL load and nonlinear load were considered and it has found that the THD of the output voltage was 1.36 % as presented in figure 11, which was lower than the one recommended by IEC and IEC62040-3 standards for the VSI in a microgrid.

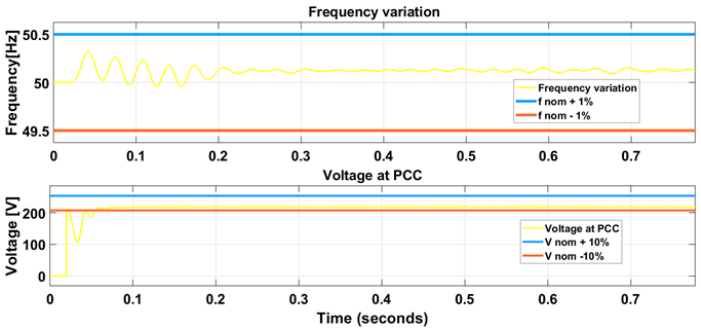

Fig. 10. Voltage and frequency variation under linear RL load conditions

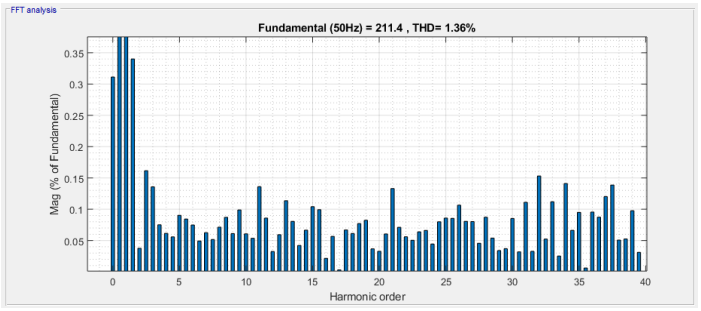

Fig. 11. The THD of the voltage during the linear load

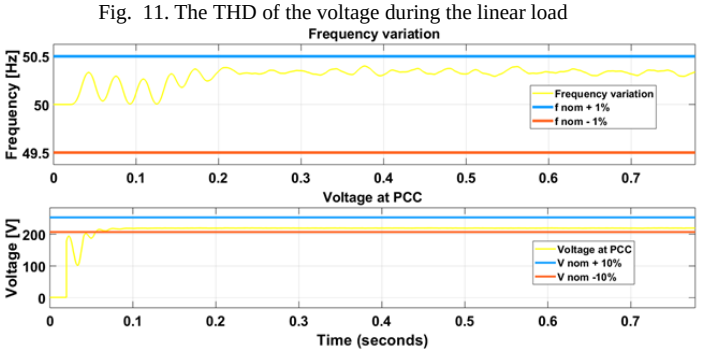

Fig. 12. Voltage and frequency variation under nonlinear load

B. Load transient analysis

During operation, a linear RL load of R=33 ohms and L=7mH was connected. Figure 13 demonstrates the system's transient behavior under the change in load from 100% to 0% and 0% to 100%. At the time t=0.1s the entire load was removed from the network, and at t=0.11s the maximum load was reconnected to the network. As shown in Figure 13 from the output current and voltage waveforms of the system, they changed with the load.

However, the output voltage of the system during transients, was a bit distorted and in a short period returned to a stable state. It showed a voltage spike at time t=0.1 s when the load was removed from the AC bus. The maximum spike value was around 241V. According to EN 50160, the allowable deviation in low voltage networks for voltage and frequency should remain in the range of +/-10% and +/-1% respectively. Figure 14 shows the frequency variation during the transient behavior, it shows that the frequency is well controlled and is kept in the range of (50.3Hz - 49.8Hz). The voltage was kept in the bounds of +/- 10% even if there is a load change.

International Journal of Engineering Research & Technology (IJERT)
ISSN: 2278-0181
Vol. 9 Issue 04, April-2020

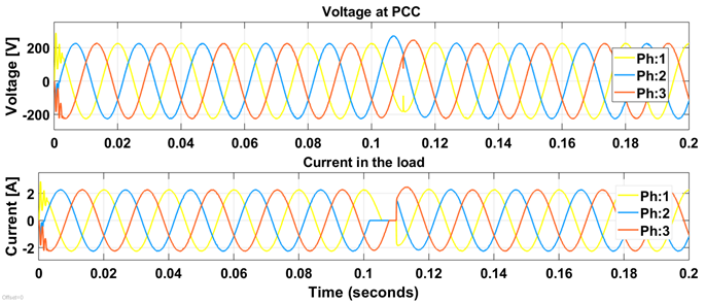

Fig. 13. Voltage / current waveforms in step-change conditions

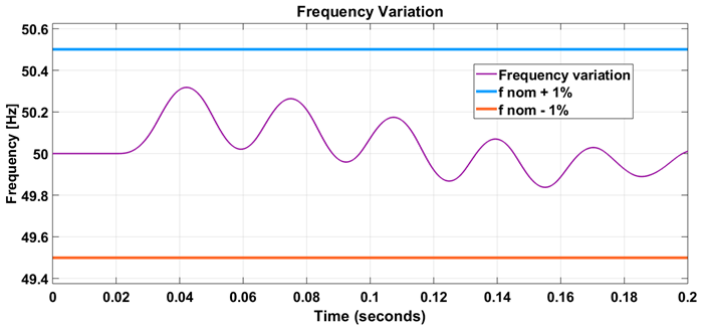

Fig. 14. Frequency variation during step change of load

An incremental change of the linear load has been done at t = 0.5, the data $R_{o1} = 40\Omega$, $L_{o1} = 1.8\,mH$ and $R_{o2} = 50\Omega$, $L_{o2} = 2\,mH$, have been used to check the performance of the controller. As can be seen, the controller stabilizes the voltage as well as the frequency both for linear load and nonlinear load as shown in figures 15-17.

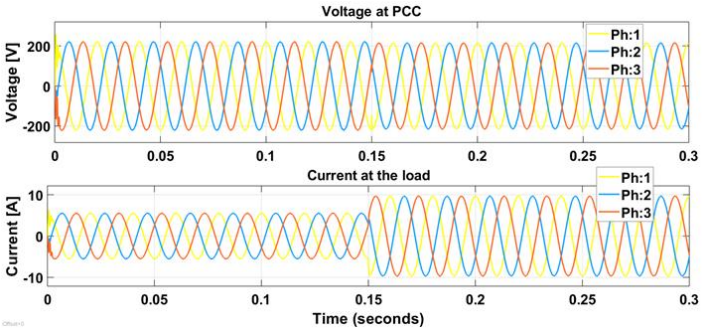

Fig. 15. Voltage and current during an incremental change of linear load

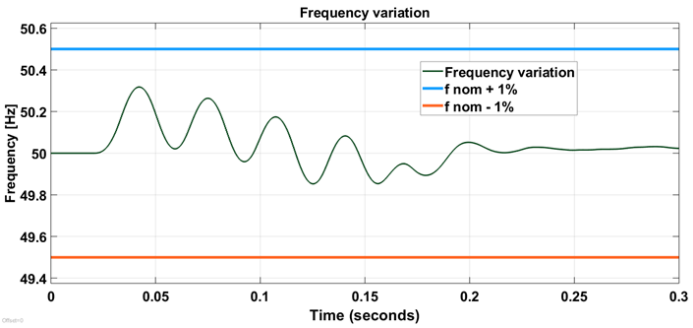

Fig. 16. Frequency variation during step change of linear load

The voltage and current waveforms display the efficacy of the proposed controller in case of nonlinear load

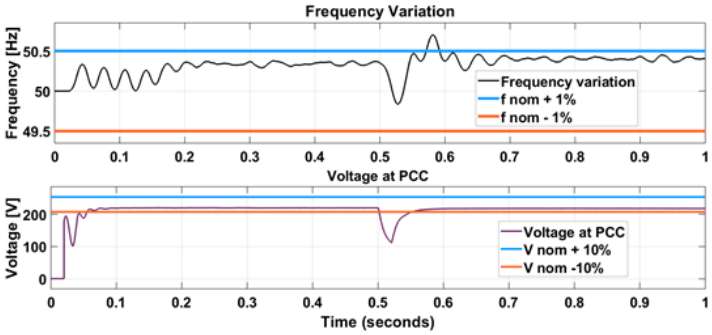

Fig. 17. Voltage and frequency variation during an incremental change of nonlinear load

C. Multiple VSI Systems

Two Voltage sources inverters have been connected as indicated in figure 1, the proposed control strategy was tested for its effectiveness in the indicated scheme. At the time t = 0.3 s, the load on the network doubled automatically, both the VSI improved their electricity output to fulfill the load demand. Figure 18 shows the VSI1 and VSI2 output voltage and load current. It was observed that the load was met by both inverters at t = 0.3 s increased in demand and the voltage slightly varied where the voltage variance was 218 V before the load change and 217 V after the load change as seen in figure 18. The waveforms voltage and the total load current at PCC are shown in figure 19, it was observed that the two currents provided by both VSIs were found to be the combined output current supplied by the two VSIs.

In Figures 20-21, power-sharing between the inverters is illustrated, where active and reactive control is exchanged evenly by the VSIs. It's found that according to EN 50160 the proposed control strategy keeps the voltage and frequency in its usual range of variability.

Figure 23 shows the variation of frequency and the signal statistics show that the RMS value is 50.03 which explains the capability of the controller for frequency control. Figure 22 highlights the THD of 3.66% for voltage signals, which is below the recommended value according to IEC62040-3 and EN 61000-2-2.

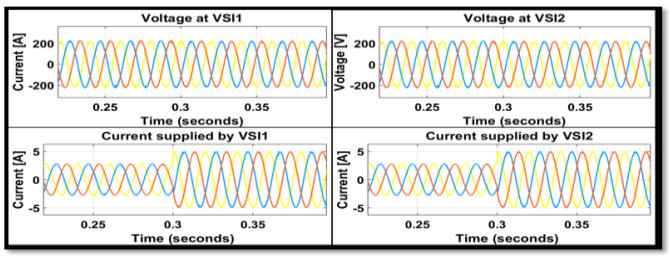

Fig. 18. VSIs' output waveforms for voltage and load current

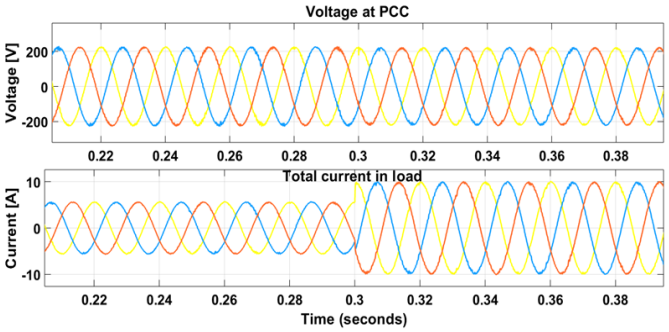

Fig. 19. Waveforms output voltage at PCC and total load current

International Journal of Engineering Research & Technology (IJERT)
ISSN: 2278-0181
Vol. 9 Issue 04, April-2020

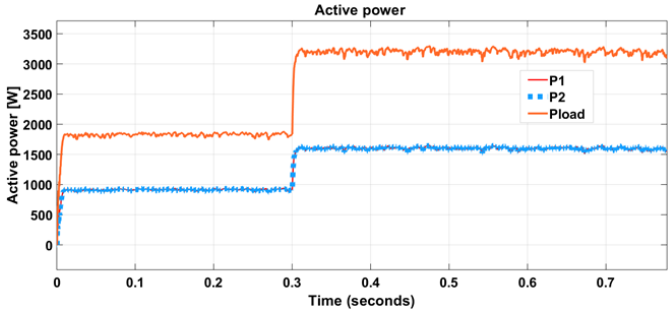

Fig. 20. Active power-sharing between VSIs with RL load

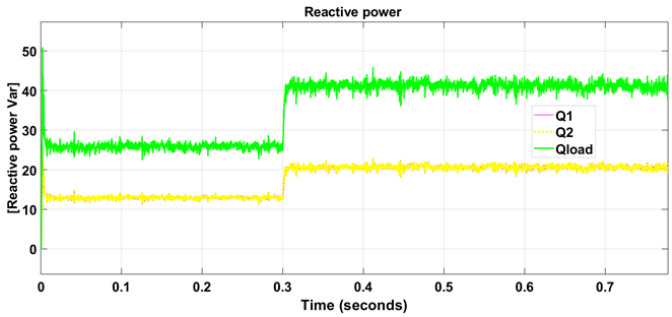

Fig. 21. Reactive power-sharing between VSIs with RL load

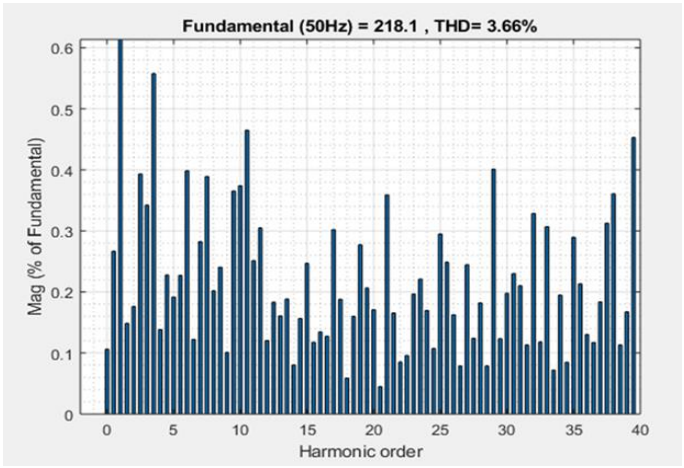

Fig. 22. The THD of the voltage at the load

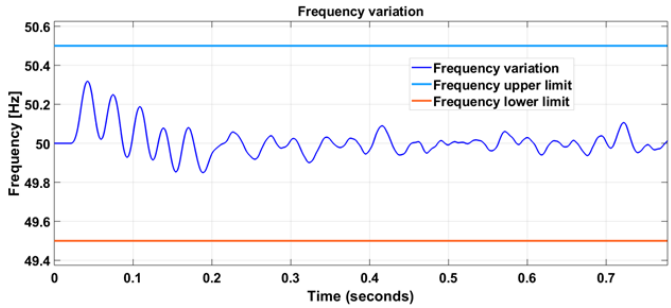

Fig. 23. Frequency variation

V. CONCLUSION

This paper suggests a technique to monitor a multi-source microgrid since each DG's key voltage is controlled by MPC. The virtual resistance droop control is used to regulate the DG's power output and ensures that the power is exchanged correctly and proportionally in an islanded mode. The results obtained suggest that the restorative loop strategy has a better improvement of micro-grid operation and can reduce the frequency and voltage amplitude fluctuations. The suggested MPC-based droop control demonstrated better performance in steady and transient conditions and also had excellent results with THD voltage signals in compliance with standards EN 61000-2-2 and IEC62040-3.

REFERENCES

[1] A. El, M. Bouzid, and P. Sicard, "Simulation of Droop Control Strategy for Parallel Inverters in Autonomous AC Microgrids," *8th Int. Conf. Model. Identif. Control*, pp. 701–706, 2016.

[2] N. Pogaku, M. Prodanović, and T. C. Green, "Modeling, analysis, and testing of autonomous operation of an inverter-based microgrid," *IEEE Trans. Power Electron.*, vol. 22, no. 2, pp. 613–625, 2007.

[3] S. Barsali, M. Ceraolo, P. Pelacchi, and D. Poli, "Control techniques of dispersed generators to improve the continuity of electricity supply," *Proc. IEEE Power Eng. Soc. Transm. Distrib. Conf.*, vol. 2, no. c, pp. 789–794, 2002.

[4] H. Shehadeh, "Inverter-Based Distributed Generators, Modeling, and Control, "*Masters' thesis submitted to D. D. I. Energia, I. Dell, and I. E. Mod*, 2017.

[5] Q. C. Zhong and Y. Zeng, "Universal Droop Control of Inverters with Different Types of Output Impedance," *IEEE Access*, vol. 4, pp. 702–712, 2016.

[6] Y. O. Choi and J. Kim, "Output impedance control method of inverter-based distributed generators for autonomous microgrid," *Energies*, vol. 10, no. 7, 2017.

[7] H. Gu, D. Wang, H. Shen, W. Zhao, and X. Guo, "New Power-Sharing Control for Inverter-Dominated Microgrid Based on Impedance Match Concept," *Sci. World J.*, pp. 1–7, 2013.

[8] A. El Boubakri, "Analysis of the Performance of Droop Controlled Inverters in Mini-Grids," *Masters' thesis submitted to Concordia University*, April 2013.

[9] Gao, D., Jiang, J. & Qiao, S. "Comparing the use of two kinds of droop control under microgrid islanded operation mode," *Archives of Electrical Engineering*,vol.62, pp.321–331,2013.

[10] U. B. Tayab and Q. M. Humayun, "Enhanced droop controller for operating parallel-connected distributed-generation inverters in a microgrid," *J. Renew. Sustain. Energy*, vol. 10, no. 4, 2018.

[11] A. J. Babqi and A. H. Etemadi, "MPC-based microgrid control with supplementary fault current limitation and smooth transition mechanisms," *IET Gener. Transm. Distrib.*, vol. 11, no. 9, pp. 2164–2172, 2017.

[12] T. Dragicevic, "Model Predictive Control of Power Converters for Robust and Fast Operation of AC Microgrids," *IEEE Trans. Power Electron.*, vol. 33, no. 7, pp. 6304–6317, 2018.

[13] L. Ruiming and W. Shengtie, "Power distribution of parallel converters in islanded microgrid using virtual resistance droop control," *Proc. 13th IEEE Conf. Ind. Electron. Appl. ICIEA 2018*, pp. 1671–1675, 2018.

[14] X. Wang, J. M. Guerrero, Z. Chen, and F. Blaabjerg, "Distributed Energy Resources in Grid-Interactive AC Microgrids," 2nd International Symposium on Power Electronics for Distributed Generation Systems, PEDG 2010, pp.806–812, 2010.

[15] K. De Brabandere *et al.*, "A Voltage and Frequency Droop Control Method for Parallel Inverters," *IEEE Trans. Power Electron.*, vol. 22, no. 4, pp. 1107–1115, 2007.

[16] X. Wang, Y. W. Li, F. Blaabjerg, and P. C. Loh, "Virtual-Impedance-Based Control for Voltage-Source and Current-Source Converters," *IEEE Trans. Power Electron.*, vol. 30, no. 12, pp. 7019–7037, 2015.

[17] I. Qing-Chang Zhong, Senior Member, "Robust Droop Controller for Accurate Proportional Load Sharing Among Inverters Operated in Parallel," *IEEE Trans. Ind. Electron.*, vol. 8, no. 4, pp. 223–241, 2000.

[18] J. M. Guerrero, J. C. Vasquez, and R. Teodorescu, "Hierarchical control of droop-controlled DC and AC microgrids - a general approach towards standardization," *Ind. Electron. 2009 IECON 09 35th Annu. Conf. IEEE*, vol. 58, no. c, pp. 4305–4310, 2009.